Activated carbon from pumpkin seeds: Production by simultaneous carbonization activation for occupational respiratory protection

Walquíria Joseane da Silva[1], Nivaldo Freire de Andrade Neto[1+], Carlos Alberto Paskocimas[1], Juan Alberto Chaves Ruiz[2], Fabíola Correa Carvalho[2], Elson Longo[3], Fabiana Villela da Motta[1], Maurício Roberto Bomio Delmonte[1]

1. Federal University of Rio Grande do Norte, Department of Materials Engineering, Natal, Brazil.
2. SENAI Institute for Renewable Energy Innovation, Natal, Brazil.
3. Federal University of São Carlos, Center for the Development of Functional Materials, São Carlos, Brazil.

+Corresponding author: Nivaldo Freire Andrade Neto, Phone: +55 84 33422406, Email address: nfandraden@gmail.com

ABSTRACT: Activated carbon materials are derived from carbonaceous sources and used as a technological element for various industrial purposes. These materials are present in most filters (cartridges) in personal respiratory protective equipment. Due to this context and to enhance sustainability concepts and human health in the production of materials, this study aimed to produce activated carbon from an abundant agricultural waste in the northeast Brazil through a route that not only favors its simultaneous carbonization and activation but also its thermal neutralization. The precursor biomass was characterized by particle size analysis, a standard testing method for moisture and ash content which were characterized by FRX, CHN, and thermal analysis. The produced activated carbon was characterized by potential of hydrogen (pH), XRD, BET, SEM, TPD by ammonia and UV-Vis analysis. The activated carbons showed yields between 73 and 78%. The morphology varied in function of the biomass interaction with the type and concentration of acid used. The produced samples showed adsorption capacity and selectivity to ammonia gas.
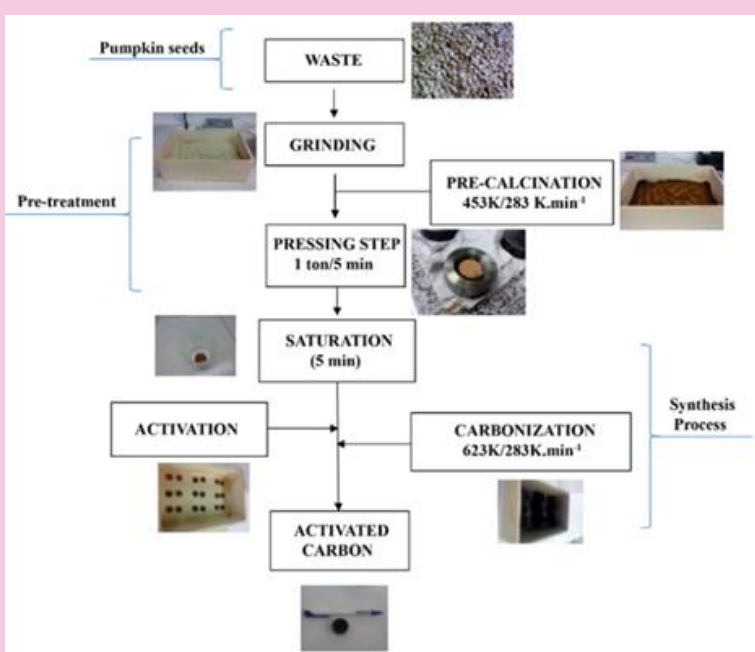
1. Introduction

Occupational respiratory protection (ORP) is often a legal requirement in some countries to guarantee the health and safety of thousands of workers who are exposed to harmful substances which may cause occupational diseases by inhaling contaminated air in the workplace. Appropriate respirators shall be used when engineering control measures are not feasible, are being implemented, evaluated, or in emergency cases (Connor *et al.*, 2016). Respirators are specific personal protective equipment designed to provide respiratory protection (MacIntyre *et al.*, 2014). Protection of some respirators occurs by removing contaminants from the air: respirators of this type include particulate respirators, which filter out airborne particles (Connor *et al.*, 2016). They have activated carbon inside their filters (cartridges) and their classification type can vary according to the risk agent to be absorbed.

Activated carbon is any carbonaceous material with favorable characteristics for adsorption reactions: well-developed internal surface area, pore structure, and superficial functional groups (Pezoti *et al.*, 2016; Poinern *et al.*, 2011) used as an adsorbent, catalyst, catalyst support, and energy storage (Shen *et al.*, 2014). On the other hand, activated carbon can also be used as an active surface to be doped or combined with other elements in a wide possibility for industrial applications (Shen *et al.*, 2014). Easy operation, large-scale production, high efficiency, sensitivity to toxic substances, and the possibility of reuse favors using activated carbon in the adsorption process (Shen *et al.*, 2014).

Activated carbons produced from biomass residues have been an important research area. Agricultural biomass and industrial waste have been used as raw material in the preparation of activated carbon (Pezoti Junior *et al.*, 2014) to find abundant, renewable, and low-cost precursors in contrast to the high production costs on an industrial scale and because of the use of nonrenewable sources of activated commercial carbons (Nunes *et al.*, 2015). Various types of waste and biomass have recently been processed to obtain activated carbon for several industrial purposes such as coconut shells (Nunes *et al.*, 2015), macadamia nuts shells (Martins *et al.*, 2014), bamboo (Shengsen Wang *et al.*, 2015), peach and olive pits (Tsyntsarski *et al.*, 2015), pineapple (Mahamad *et al.*, 2015), peanut shells (Zhang and Lu, 2015), rice husks (Dalai *et al.*, 2015), sugarcane bagasse (Dalai *et al.*, 2015; Gonzaga *et al.*, 2018), sewage sludge (Huang *et al.*, 2017; Wu *et al.*, 2014), waste from palm tree stems (AlOthman *et al.*, 2014), seeds from *Platanus*

orientalis biomass (Dodevski *et al.*, 2017), and banana peel (Van Thuan *et al.*, 2017), among others.

Pumpkin is a typical fruit in northeastern Brazil. Oil extraction from its seeds does not have any significant productive or technological relevance in the region. Therefore, when these seeds are not reused for planting, they are either intended for human and animal consumption just because of the beneficial nutrients they contain (Carvalho *et al.*, 2012) or are discarded (Joshi *et al.*, 1993). Thus, it is a by-product of the agricultural segment with low technological and commercial impact. Traditional methods to produce activated carbon propose the carbonization of biomass followed by the use of activators (whether chemical or physical or a combination of both) in two asynchronous different steps (Gonçalves *et al.*, 2016; Solís-Domínguez *et al.*, 2011). An improvement in the production process has recently been considered so that these steps occur simultaneously. This process is classified as a synchronous one-step process. As a result, the characteristics of the obtained material vary according to these production steps.

Thus, this paper aimed to synthesize activated carbon from pumpkin seeds using the carbonization route and chemical activation by thermal neutralization. The relationship among the synthesis methodology, reagents, and starting materials used with the characteristics shown by the activated carbon was investigated. Adsorption experiments with TPD were carried out with ammonia in the presence of moisture. It became an agent which carried risks caused by accidental inhalation, which is harmful to people's health in working conditions in all industries where it is employed. Moreover, the adsorption potential of aqueous solutions of methylene blue dye was investigated following the ultraviolet-visible (UV-Vis) measurements in the absorbance model. Furthermore, this investigation may demonstrate the effectiveness of the produced material for environmental applications, human health, and removing pollutants from wastewater.

2. Experimental

2.1 Characteristics

The plant which originates pumpkin belongs to the *Cucurbita* genus (Cucurbitaceae family) (Hameed *et al.*, 2008) and comprises various wild and domesticated species native to the Americas. The plant grows well in hot and dry climates (Ferreira *et al.*, 2017). Pumpkin has flat edible seeds (Njoku *et al.*, 2014).

2.2 Characterization of the biomass

The pumpkin seeds were fragmented into a food commercial crusher for 7 min at 400 W of power and (55 ± 5) Hz. The material was deagglomerated using a 200-mesh sieve. The fragmented seeds were then characterized by particle size analysis using laser diffraction, the standard testing method for moisture and ash content, X-ray fluorescence (FRX), elementary chemical analysis (CHN), and thermal analysis. The distribution curve of the particle size analysis by laser diffraction carried out in the waste was obtained by granulometry in a CILAS 1180 device in an aqueous liquid dispersant, and then subjected to the effects of ultrasonic agitation for 60 s. The standard testing method for moisture and ash content was performed according to ASTM E1755 and E1756, respectively.

Chemical composition was obtained by FRX spectroscopy using an EDX-720 Shimadzu in a vacuum atmosphere. Elementary chemical analysis was performed with 2.7 mg in a Pekin Elmer analyzer 2400 Series II model connected to a microbalance model AutoBalance controller. Helium gas (18 psi – 900 mL min⁻¹– 913 K) and oxygen (15 psi – 50 mL min⁻¹ – 1198 K) were used.

A thermal analysis was performed in a Netzsch STA Model 449F3 device at a heating rate of 283 K min⁻¹ and a temperature range of 303–1023 K using 10 mg of the sample under synthetic airflow (100 mL min⁻¹).

2.3 Pretreatment

The precalcination of biomass was performed at 453 K with an isotherm of 1 h and a heating rate of 283 K min⁻¹ in a Linn Elektro Therm furnace. Next, the material was pressed into pellets in a stainless-steel matrix in a ratio of 0.3:1 of binder/raw material using 1 Ton for 5 min. Pellets were fabricated in a cylindrical shape of approximately 25 mm in diameter by 5 mm high.

2.4 Synthesis

The samples were produced by the carbonization reaction and concomitant to chemical activation. Three different acids were used in this process: hydrochloric (CLO), sulfuric (SUL), and nitric (NIT) acids in different concentrations (10%, 30%, 50% in acid:water volume, respectively) for chemical activation. This method was applied according to the following procedure: each pellet obtained (after the pretreatment) was put in an acid solution for 5 min until complete saturation and placed directly into a mullite-cordierite box. The pellets were covered with precalcined raw biomass. The box was immediately closed and heated to 623 K at a heating rate of 283 K min⁻¹ in an air atmosphere for 10 min. The method is illustrated in the flow chart demonstrating the experimental procedure as shown in Fig. 1. Thermal neutralization was applied to the obtained activated carbons: the samples were heated between 573–673 K for 144 h and then cooled at room temperature. The pellets were deagglomerated in an agate mortar.

The nomenclature used to identify the samples were PS (pumpkin seeds) plus the abbreviation of the employed acid + amount (%) of activator used. This nomenclature was used for different amounts of acids and concentrations.

2.5 Characterization of activated carbons

The following techniques were used to characterize active carbons: potential of hydrogen (pH), X-ray diffraction (XRD), specific surface area using BET (Brunauer-Emmett-Teller), and scanning electron microscopy (SEM), temperature-programmed desorption (TPD) by ammonia and UV-vis spectrometer. The pH measures were performed in a diluted aqueous solution with deagglomerated powders of activated carbon produced in a mass ratio of 1:1 (water:sample) under stirring for 10 min at room temperature (298K). The solution was filtered and measured by the electrometric method using a Hanna PH21 digital meter with a measuring range of 0–14, resolution of 0.01, an accuracy of $\pm$ 0.02, and HI 1110 electrode type. XRD diffractograms were performed by a Shimadzu XRD-7000 diffractometer, CuKα monochromatic radiation, with an angular range of 2θ range from 10 to 80°, scanning speed of 1° min⁻¹, a step of 0.02°, a voltage of 40 kV and a current of 30 mA. The specific surface area measurements were obtained by a Quanta Chrome Corporation NOVA model-2000 using the BET method. The samples were previously degassed at 473K for 1 h. The SEM micrographs were obtained using a Hitachi High-TM3000 microscope. The samples were directly deposited into a metallic holder coated with carbon to fix them.

TPD by ammonia was performed in the automated analyzer Micromeritics AutoChem II 2029. TPD runs occurred with approximately 0.100 g of material at a flow of 50 mL min⁻¹ of helium gas at ambient temperature up to 383 K (heating rate of 283 K min⁻¹), and then up to 573 K. It was then cooled down to 323 K. After 1 min, a gaseous mixture of ammonia and helium

(5% NH$_3$/He) with a flow rate of 50 mL min^{-1} was introduced for 30 min under the same heating rate. Thereafter, the inert gas recirculated in the system at the same flow rate, and the sequence of the described process was repeated by heating at 373 K (283 K min^{-1},

15 min) and 573 K (283 K min^{-1}, 20 min). The UV-vis spectrometer was performed using a Shimadzu UV-2600 spectrophotometer at a wavelength range between 400 and 800 nm.
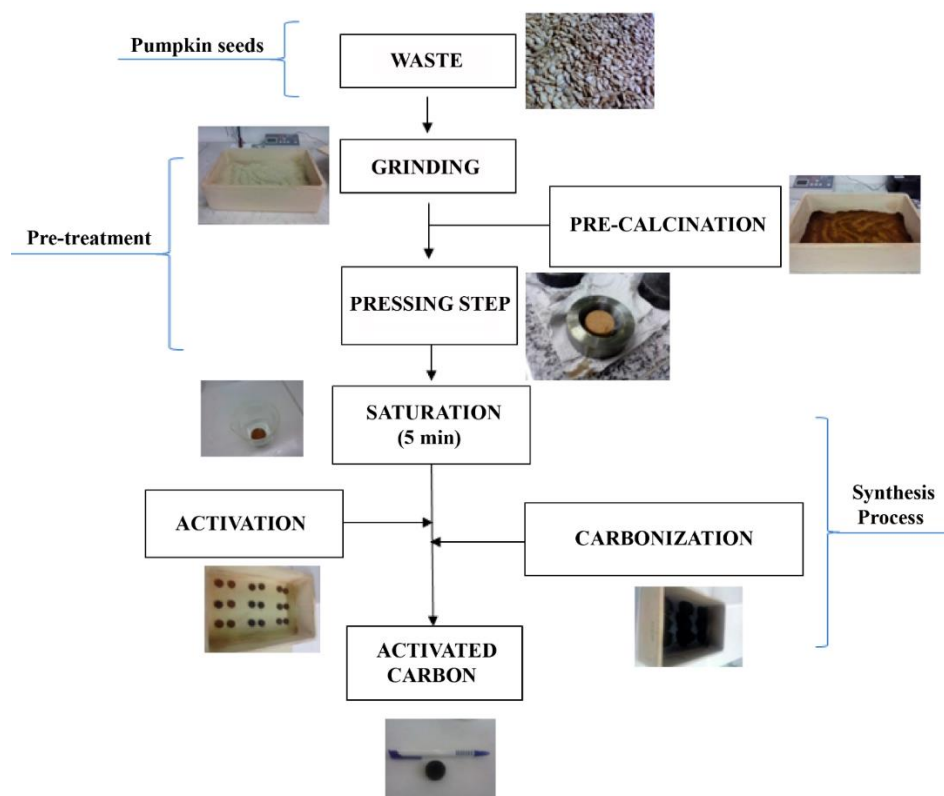

Figure 1. Flowchart of the experimental production procedure for the activated carbon.

3. Results and Discussion

3.1 Characterization of the precursor biomass

Waste processing in the fragmentation and burning processes was achieved by reducing the particle size through grinding, which provided a more homogenous and uniform characteristic to the raw material. The intrinsic characteristics of the raw material determined the type of grinding used, and therefore conditioned its grinding evolution. The oleaginous nature of the seeds which are sensitive to high temperatures made the traditional use of fragmentation equipment unfeasible. This justified the use of commercial crushers as described in the methodology.

The result of particle sizes of the powder obtained after waste fragmentation in natura is shown in the granulometric distribution curve in Fig. S1 (Supplementary Information). The sample shows a wide variation in the particle size, irregular visual appearance,

and wide distribution range between 2.5 to 550 mm. The average particle size measured is about 59.75 mm. Enlargement in the size distribution technique suggests the presence of rough particles with an irregular shape that is not perfectly spherical, according to the principle of the technique and the Fraunhofer Theory (Beuselinck et al., 1998).

After the grinding process, the in natura samples have a level of humidity and ash of 0.10% and 10.44%, respectively. It is known that the presence of moisture in biomass is related to the intrinsic characteristics of the waste such as aspects of cultivation, storage, and production steps, or their combination with each one of the factors. The presence of inorganic impurities is relatively higher than the humidity (only 0.1%), which can indicate a waste that is less saturated with reduced hydration. This may lead to the mass loss being minimized by humidity.

The gravimetric variation which represented the standard result and was adapted from the ash content is shown in Fig. 2. A reduction in the isotherm time for

preserving the thermal stability of the waste during the test ash content did not significantly affect the results. This was one of the viable ways for the variations which were noted to obtain the constant mass. The residue (0.0922 g) quantities were measured after measuring about 10.44% of the ash content. This percentage represents the amount of the remaining mineral part and impurities after degradation of the organic matter after the test and may have a predominant composition by potassium, phosphorus, sulfur, and sodium as shown in the FRX results of the in natura sample (Tab. 1). The presence of alkali metal oxides, alkaline earth metal, and others with less significant quantities is also observed, which can interact with the activator acid during the carbonization-activation process, thereby causing over-position phases without necessarily exerting a strong influence on the material properties due to the low amounts detected. Evaluating the ash content can represent a measure of minerals and other inorganic materials and possible impurities present in the in natura sample of the pumpkin seeds according to the testing method.
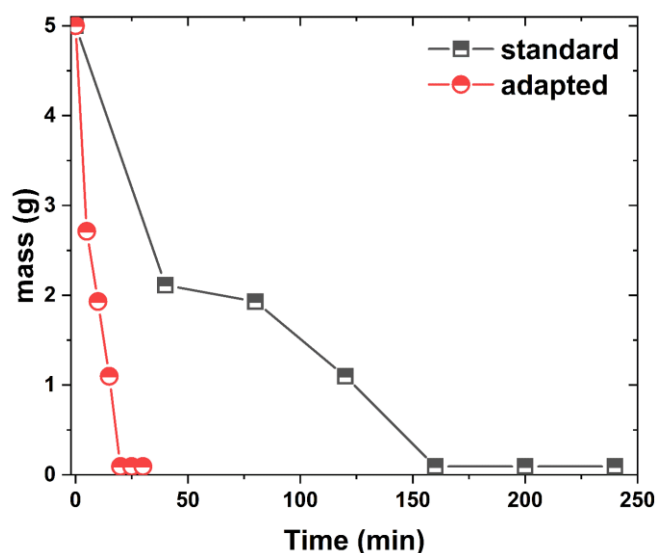
Table 1. Chemical composition of the in natura sample.

Chemical composition	In natura sample (%)
K_2O	41.67
P_2O_5	18.61
SO_3	14.73
Na_2O	11.41
CaO	3.07
Fe_2O_3	2.92
SiO_2	2.46
ZnO	2.21
CuO	1.12
MnO	0.97
Rb_2O	0.83

Table 2. Mean values of the CNH composition of PS samples used in this work in comparison with a commercial sample. In which: PS^1 = in natura sample and PS^2 = sample used in the standard test method for ash content.

Samples	Carbon (%)	Hydrogen (%)	Nitrogen (%)
PS^1	55.64	9.81	5.88
PS^2	40.64	2.45	9.99

The thermal characterization of in natura PS is shown in Fig. 3. The thermal decomposition occurs in four mass variation steps directly related to the composition of the *Cucurbita* seeds, which are rich in oil, protein, fiber, and micronutrients (Joshi *et al.*, 1993). The mass loss that occurs at approximately 383 K can be attributed to moisture, in turn, related to water removal (Caputi *et al.*, 1991). Next, the second event had a 40.83% weight loss in the range of 415 to 620 K and can be associated with the degradation of the organic matter and with the formation of carbonized material. The third stage occurs quickly at the moment that the temperature reaches a maximum of 653 K with 14.31% weight loss which may be related to the combustion of oils. The fourth decomposition stage occurs between 695–937 K corresponds to 31.66% weight loss which decomposes slowly and may be attributed to protein degradation and thermal decomposition of the other micronutrients. The residue is stable at 923 K and showed a mass change of 7.43%. These results show a reduction of the humidity values and differential thermal stability to the normative parameters applied to biomass in this work. Thus, the standard tests and thermal analysis of biomass were fundamental to achieve a carbonization temperature that was favorable to producing the activated carbon.

Figure 2. Comparative analysis of the weight loss of in natura ground samples during the ash content test for the standard and adapted samples.

The amount of volatile matter was quantified by elemental chemical analysis in two test runs. The carbon, nitrogen, and oxygen percentages measured in the analyzed samples are shown in Tab. 2. The difference in the carbon percentage between the PS in natura sample and the PS charred sample is very subtle and not significant, which may indicate that all the carbon mass was substantially preserved during the process proposed in this work.
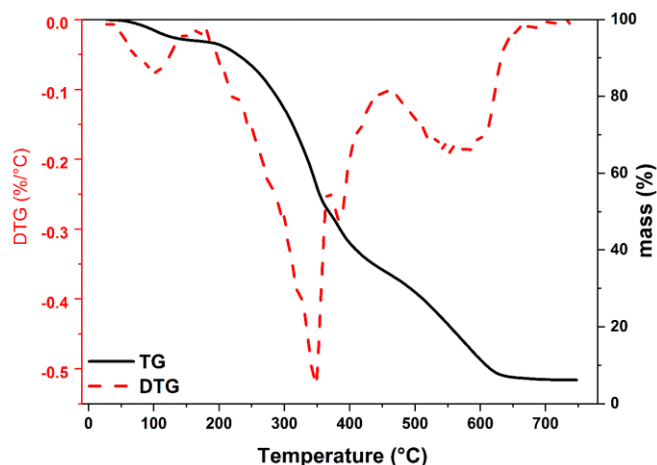
Figure 3. Thermal analysis curves (TG-DTG) of the in natura PS sample.

From the heat treatment applied to obtain the activated carbon, the ignition and activation temperatures are 563~583 and 623 K, respectively. In addition, the gravimetric yield of the powdered and palletized material was 21.93 and 61.41%, respectively. The gravimetric yield in this study was calculated from the ratio of the produced carbon mass and biomass precursor, according to Eq. 1.

$$R\ (\%) = (\text{produced carbon (mass)/biomass (mass)}) \times 100 \qquad (1)$$

The yield is the determining factor to control the burning and production process. In this sense, it is a variable that indicates the carbonization efficiency in a process given as a percentage. The carbonization temperature and combustion efficiency are also influenced by other factors such as humidification and volatile content which affect the calorific value of the sample. It was also observed that the yields were variable depending on their morphological aspect. The performance was higher when the sample was compressed into a pellet form. Therefore, the processing proposed in this study included the precarbonization together with the pressing procedure. The aim was to minimize the mass loss by moisture and eliminate other components volatilized at 453 K with the precarbonization stage. This was used to increase the carbonization efficiency and enable the process on an industrial scale because the performance in powder form will be low due to the gravimetric yield having little significance when compared with the yields shown in the pellet form.

The percentage value of the burn-off is implicit in the results of the gravimetric yield of activated carbon pellets because the carbonization occurred simultaneously to activation. This understanding becomes clearer with the yield definition given by Marshall *et al.* (2000), which defines it as the amount of the precursor remaining after pyrolysis and activation. Thus, the total yield of the activated carbon pellet values depends on the activator and proportions used. These results are shown in Tab. 3.

Table 3. Total gravimetric yield of activated carbons according to the activator proportions.

Sample	Total gravimetric yield (%)
PSCLO10	75.94
PSCLO30	80.78
PSCLO50	66.76
PSNIT10	78.00
PSNIT30	78.98
PSNIT50	74.36
PSSUL10	67.82
PSSUL30	76.82
PSSUL50	73.04

Yields vary slightly depending on the activator used. Although it had high and low peaks for the PSCLO30 and PSCLO50 samples, others had yields between 73 and 78%. The analysis of each group demonstrates an increase in the yield in the ratio of 30% activator, and a fall when the activator had a concentration of 50%. However, they are superior to the mean measured in the gravimetric yield of the carbonized pellets (on a dry basis without the activator) in all cases. Another variable observed in this phase was the firing atmosphere, which influences carbonization. As described in the methodology, it was decided to maintain a powder-air bed which provides a reducing atmosphere. This use is also a factor that enables the process on an industrial scale, thereby allowing carbonization in large amounts, avoiding the use of reducing atmospheres, and simplifying the process at a low cost. The powder-air bed can be discarded if the mass ratio is considerably higher than for the available oxygen.

3.2 Characterization of activated carbons

3.2.1 Structural

Literature shows that the typical procedure to produce activated carbon usually involves washing the produced material with water or using a chemical compound, or both, to promote neutralization of the proposed activation, especially when the chemical activation is applied to eliminate the remaining impregnating chemical agent (Hameed *et al.*, 2008; Rovani *et al.*, 2016). The thermal neutralization proposal was an alternative to the commonly reported

traditional neutralization methods. The measured pH values are shown in Tab. 4. The pH of the carbonized sample with no activator obtained under the same experimental synthesis conditions was also measured for comparison.

**Table 4.** pH of activated carbon solutions.

Samples	Colorimetric method	Electrometric method
OS	7	7.02
PSCLO50	6	6.99
PSNIT50	7	7.12
PSSUL50	6	6.36

Samples from the PSCLO group had very moderate acidity, quite close to neutrality. Only samples from the PSSUL group showed a relative acidity of 6.36, probably due to the presence of residual sulfur still present in the carbon structure, making the structure more stable in the proposed neutralization temperature. Therefore, this group was subjected to a new neutralization run at 723 K temperature. After this, the measured pH was around 7.09, with the value approaching neutral given the other samples and a reference sample without an activator which indicates the efficiency of the proposed neutralization. The choice of thermal neutralization over traditional means has the advantage of facilitating the manufacturing process and more viably dealing with the wastes from the process. Washing in the industrial field possibly generates residual effluent, which would constitute another step in the process of burdening deployment, maintenance costs of unit operations, and environmental responsibilities associated with it.

The XRD diffraction of PS carbonized without acid activation is shown in Fig. 4a. The PS sample revealed a typical structure of amorphous materials and types of activated carbon with a larger peak at 20.5°. This may be related to the composition of the remaining mineral part after degradation of the organic matter: mineral components are still present in the composition of the waste and/or residual impurities in a very slight amount after the treatment, but not sufficient to promote forming other stable structures with significant crystallinity under the thermal treatment conditions. The XRD of the produced activated carbons is shown in Fig. 4b. Compared to Fig. 4a, it is noted that an amorphous matrix originally occurs during pyrolysis in overlapping phases when the process is applied in full with the use of the activator simultaneously to carbonization. There was a contour profile presented by the pure carbon plus crystalline phase peaks observed in all groups which varied according to the activator. The identified phases are mixed compounds dispersed in the amorphous matrix and made up of minerals present in biomass associated with the elements of the employed acid.

Except for PSNIT samples (Fig. 4c), which showed a peak at 2q = 60° of a mixed compound that only exists when a greater amount of activator was used, but without any relative significance. The other groups retained the same profile with each other. It is seen that the activators caused the appearance of different phases in the carbonized material, generating activated carbons with diffraction characteristics depending on the activator used. Sulfuric acid was the agent that caused the greatest change in the activated carbon phases because it generated a greater number of peaks than other activators according to the PSSUL group (Fig. 4d). However, the number of dispersed phases of the amorphous base is more discreet in the other group.
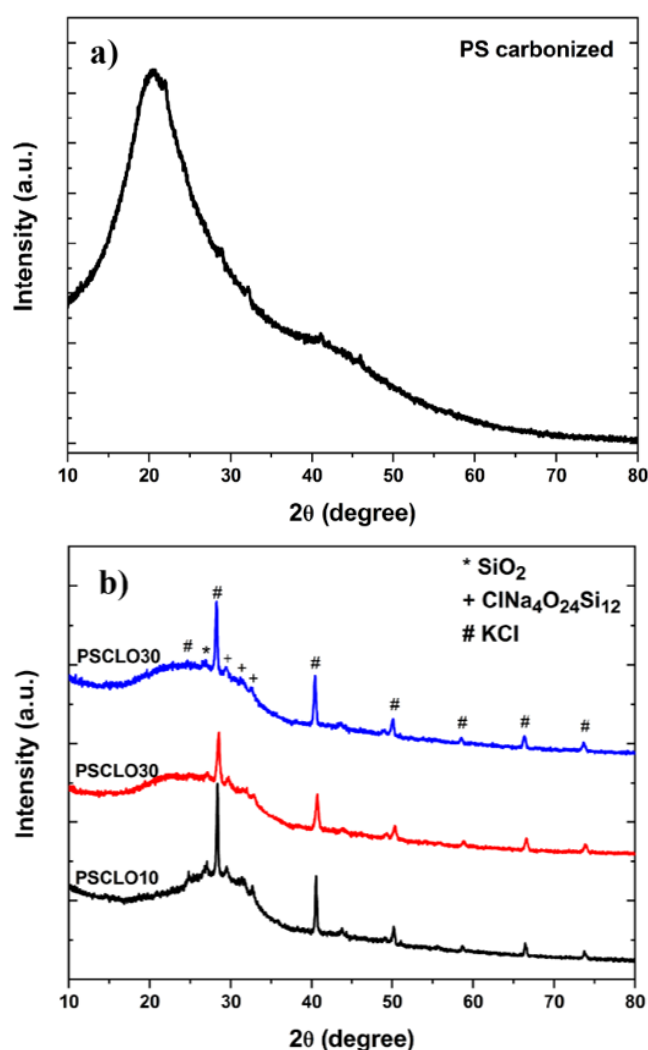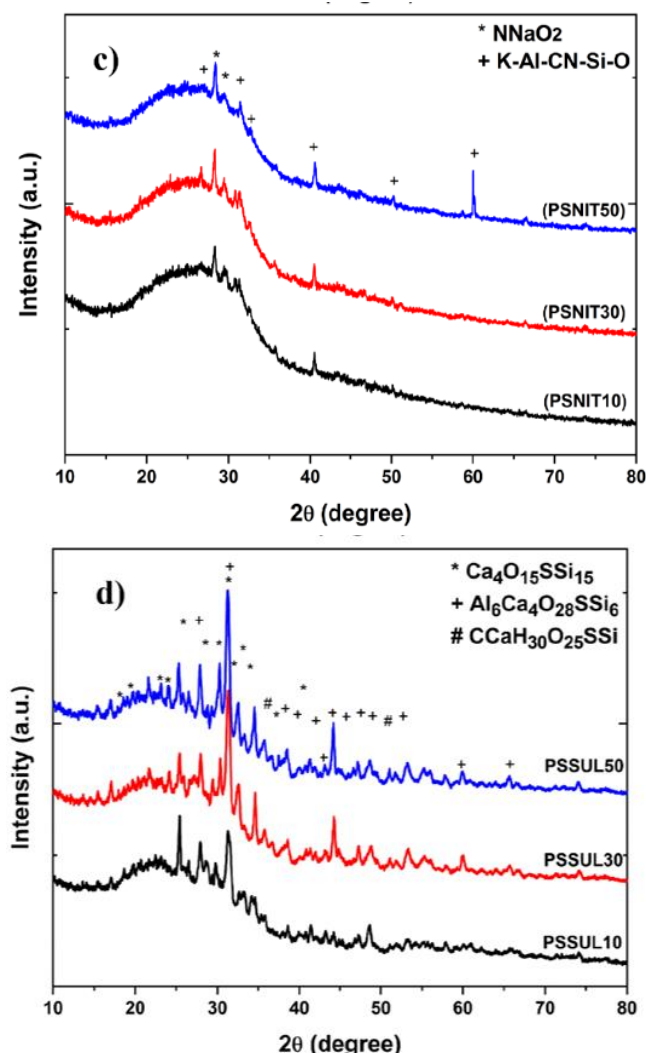
Figure 4 - X-ray diffractogram of the **(a)** carbonized PS, **(b)** PSCLO, **(c)** PSNIT and **(d)** PSSUL samples.

The XRD analysis showed that the activated carbon characteristics are associated with the composition and waste processing; when subjected to thermal excitation, it tends to eliminate organic and moisture matters, producing pure carbon or forming thermodynamically stable structures related to the presence of inorganic and/or impurities depending on the additives and/or activating elements. Thus, the activated carbon differs from the carbonized sample by the presence of phases resulting from the activator interacting and modifying the structure during processing. This enables us to infer that the activating agent reacted with the biomass during the carbonization process, and carbonization and activation consequently occurred simultaneously as proposed in this work.

The morphology of the samples was analyzed by SEM according to the images in Fig. 5. The in natura waste presented regular, equiaxed, and homogeneous morphology constituted by blocks and dense plaques with a few scattered spherical corpuscles, which are an intrinsic characteristic of the biomass (Fig. 5a). A sample was collected to check the surface texture and to prove the effects of the proposed alterations concerning the raw material due to the experimental changes applied to the test ash content. The micrograph of this sample (Fig. 5b) shows the permanence of the blocks and characteristic plaques, which in addition to not compromising the test results also caused satisfactory changes in morphology, leaving a matrix with a porous aspect about the initially characterized thick morphology. Thus, the plaques are porous with predominantly well-distributed spherical particles on the surface.

The samples submitted to the simultaneous activation and carbonization process showed different morphologies evidenced by micrographs (Fig. 5c–k). The diameter and pore volume tend to increase in the chemical activation process, and new pores are created due to the reaction between the carbon and activator (Yorgun and Yıldız, 2015). Furthermore, the presence of pores among the plaques was also favored by the simultaneous carbonization, making the biomass pyrolysis occur simultaneously to the activation. It is possible to note an increase in spaces produced by the effects of activating agents in the dense and compact matrix of the in natura waste with varying morphology depending on the activator.

The results of specific surface area (S_{BET}), medium pore diameter (D_{pm}), and the total pore volume (V_p) are shown in Tab. 5. The surface area and pore volume values for each group tended to be directly proportional to the concentration of the activator, except for the PSCLO50 and PSSUL50 samples. All the activated carbon samples produced have the same order of magnitude considering all the physical parameters measured in this test; however, the chemical activation with hydrochloric acid showed the best results.

Table 5. Typical parameters determined by BET.

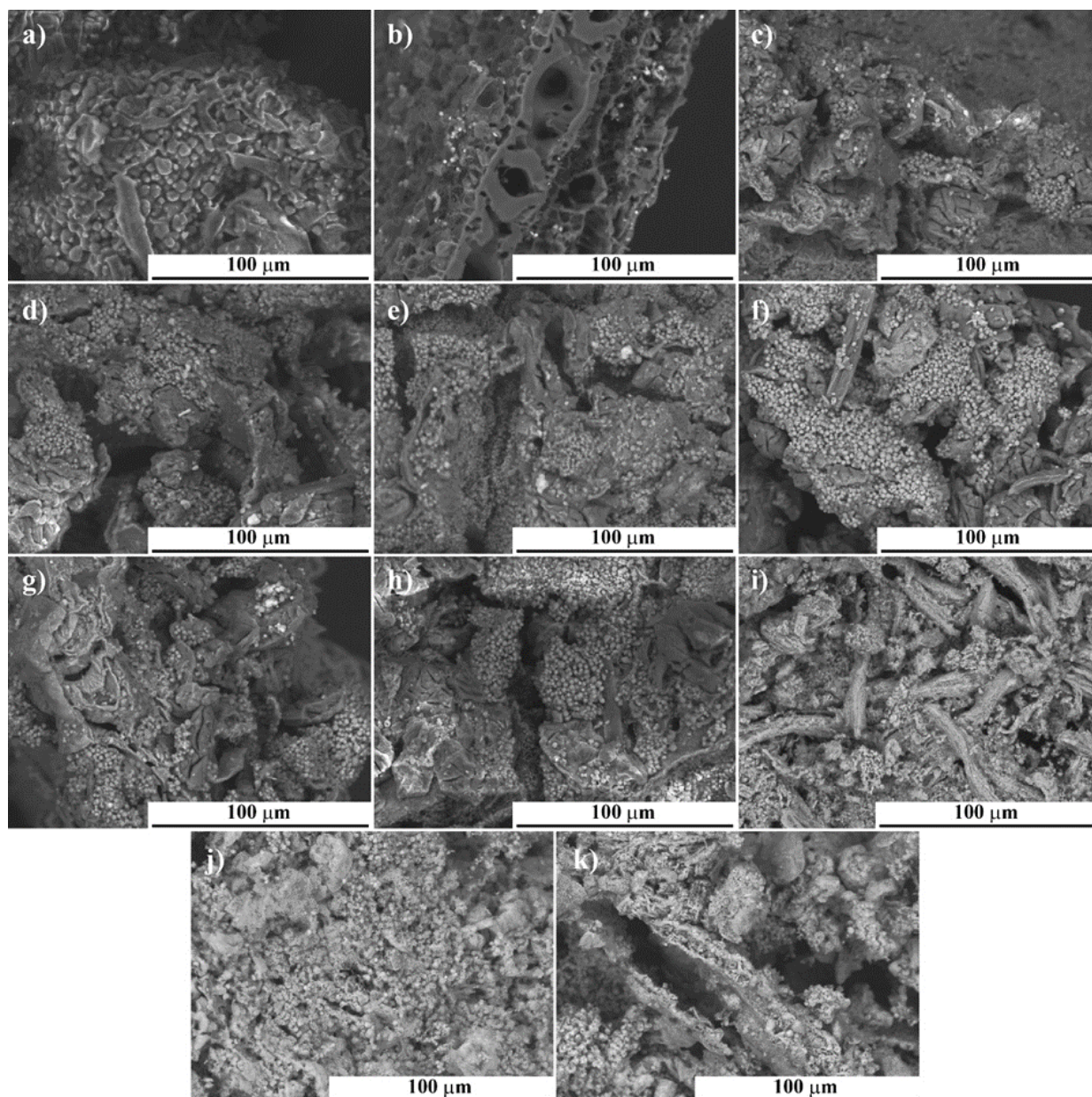| Samples	Physical parameters		
	S_{BET} (m² g⁻¹)	Vp (cm³ g⁻¹)	D_{pm} (Å)
PSCLO10	6.77	0.0035	20.68
PSCLO30	8.93	0.0045	20.58
PSCLO50	6.42	0.0033	20.77
PSNIT10	5.08	0.0025	20.35
PSNIT30	5.48	0.0028	20.44
PSNIT50	5.60	0.0028	20.09
PSSUL10	3.68	0.0016	18.43
PSSUL30	5.29	0.0027	20.59
PSSUL50	4.45	0.0022	20.50

Figure 5. SEM micrographs for the **(a)** biomass, **(b)** carbonized PS, **(c–e)** PSCLO (10, 30 and 50%), **(f–h)** PSNIT (10, 30 and 50%) and **(i–k)** PSSUL (10, 30 and 50%) samples.

The specific area values are not only dependent on the processing applied but also influence the intrinsic characteristics of the raw material and the adsorbate. Marshall *et al.* (2000) explained that low burn-off values can lead to a low adsorption capacity by reducing the surface area. As the surface area is not related only to textural properties, it is possible that the adsorption capacity is not impaired, but also to the physical and chemical properties exhibited during adsorption.

The potential of the activated carbon adsorption is not only determined by its total surface area, but also by its inner porous structure, presence of functional groups on the pore surface, and an electrostatic charge of the adsorbent and adsorbate (Alam *et al.*, 2007). Bansal *et al.* (1989) explained that the adsorption on activated carbon is influenced by three factors: pore size, chemical structure, and active sites. The pore size determines the adsorption capacity, the chemical structure influences the interaction with polar and nonpolar adsorbates (acidic or basic surface groups), and the active sites determine the type of chemical reactions with other molecules. This may also evidence the reasons why the potential for adsorption of these samples was not compromised, as the TPD results and the UV-Vis analysis showed.

3.2.2 Application

The TPD test results show that the sample groups have profiles with only one desorption region, constituting a peak at 573 K (Fig. 6a–c). This value corresponds to the regeneration temperature of saturated activated carbon; in this case, the test with ammonia gas is appropriate to ensure that this gas is not inhaled by the user during their work as they are using respiratory personal protective equipment without saturation. A filter change is always advisable when saturation occurs from active sites, i.e., when the pores (where adsorption occurs) are completely saturated by the filtrate, reducing the potential of activated carbon and consequently compromising the adsorption capacity. This can vary due to the agent, the concentration, and exposure time of the supposedly contaminated workplace to the risk of contamination by the gaseous chemical agent.

In the case of the PSCLO group sample (Fig. 6a), the desorption profile was similar regardless of the amount of activator used in the preparation of activated carbon. The PSNIT (Fig. 6b) and PSSUL groups (Fig. 6c) showed a variation in the desorption profiles for quantities of 30 and 50%, respectively. This behavior should be directly related to the type of interaction between the acid activator and activated carbon which caused changes with increasing concentration. The amount of desorbed ammonia relative to the acid and its concentration is shown in Fig. 6d. The PSCLO group does not have any significant variations in desorption in function for the activator concentration when compared to the other groups. The adsorption had maximum and minimum peaks of 0.20 and 0.16 mol g^{-1} of ammonia in the PSCLO10 and PSCLO30 samples, respectively. The sample produced with 50% hydrochloric acid presented an intermediate value. Thus, the similarity of the TPD profiles (Fig. 6a) and desorbed volumes in this group (Fig. 6d) showed that the percentage of activator, in this case, had little influence on the number of acidic sites on the solid surface.

The interaction of activators in the PSNIT and PSSUL groups with the biomass is different and opposite to the increasing amount of acid used in the preparation of the activated carbon. It is more convenient to conduct the treatment using only 10% of the activators in all cases. The samples that showed greater amounts of desorbed NH_3 were PSNIT50 (0.24 mol g^{-1}), PSNIT10, and PSSUL30 (both 0.21 mol g^{-1}), which may indicate a greater number of acid sites, and therefore higher adsorption capacity and selectivity for ammonia gas. The UV-vis spectroscopy results are shown in the Supplementary Information in

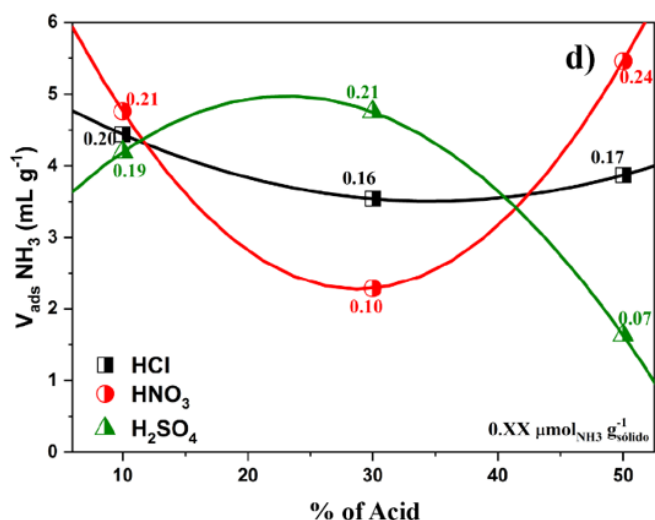this paper. The spectra show the liquid phase adsorption potential of each material tested with methylene blue dye.
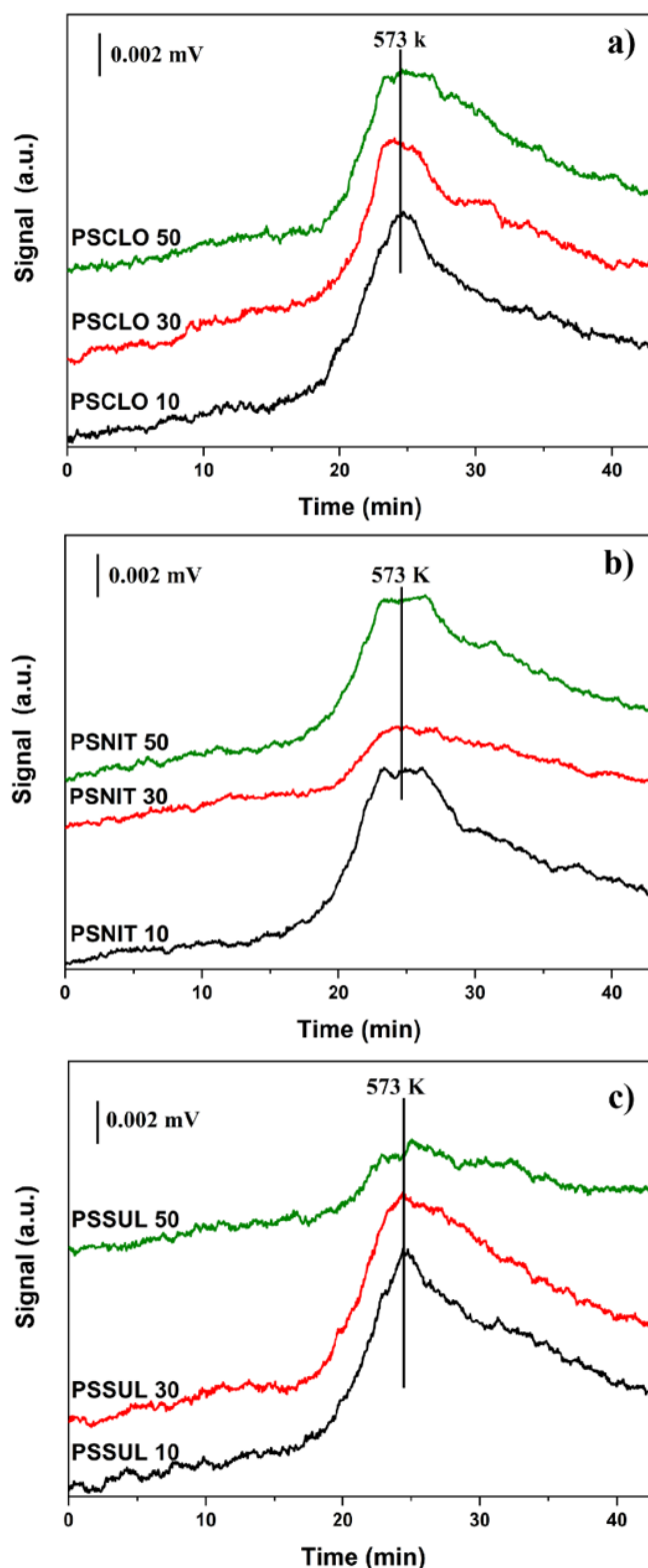
Figure 6. TPD-NH₃ profile curve for the **(a)** PSCLO, **(b)** PSNIT and **(c)** PSSUL samples and **(d)** total volumes of ammonia desorbed by the activated carbon samples.

The PSCLO and PSNIT groups had adsorption times measured every 2 min and 30 s. The adsorption reaction in the samples from the PSSUL group occurred slightly slower and was therefore measured every 5 min. After the beginning of adsorption, the spectral intervals were measured (at known time intervals) until the maximum adsorption time between the adsorbate (dye) and the adsorbent (activated carbon). There was only pure methylene blue solution at a concentration of 10^{-5} ppm at the initial time (t0). Thus, the decrease in the characteristic absorption band of methylene blue demonstrated the reactivity of the material.

In Fig. S2 (Supplementary Information), the PSCLO30 sample showed the same reaction time as PSCLO50, but PSCLO50 showed a 100% absorbance reduction with the total color reduction of the solution. Both PSCLO10 and PSCLO30 presented 97% of adsorbed dye, but PSCLO10 was consumed slightly faster. The PSCLO50 sample stood out slightly about the total degradation of the dye. The measurement of reaction time intervals was also made every 2 min and 30 s in the activated carbon samples for the PSNIT group at Fig. S3 (Supplementary Information). The highlight in this group was the PSNIT30 sample whose performance was better than the others: the dye was degraded by 95% in only 2 min and 30 s. The PSNIT10 and PSNIT50 groups showed equal reaction times (17 min and 30 s) and practically the same percentage of adsorbed dye. The total reaction time varied with the acid percentage of the activator used in the synthesis process.

The adsorption reaction times of the PSSUL group were more extensive and variable with the acid synthesis concentration, as can be seen in Fig. S4 (Supplementary Information). The best performance of this group was from the PSSUL10 sample with 99% dye degradation at 25 min, followed by the PSSUL30 with 94% at 55 min. The PSSUL50 sample reached a 50 min reaction time to degrade 89% of methylene blue dye. It was observed that acid concentration in this group was inversely proportional to the degradation performance of the dye for this group.

The adsorption reactions in the liquid phase of the PSSUL showed some instability in the concentration of the methylene blue bands along with the degradation, indicating a possible oscillation of the absorbance dye. It was observed that the dye concentration in the spectra was higher than the initial solution at some moments. The tests were repeated and the results converged at this point, probably caused by some instability in the equipment during the performed readings. Such a situation may also indicate a reversible reaction character by the kinetics and thermodynamics of the reaction with this material in the initial moments, but which tends to stabilize over time and adsorb the dye. The pore structure morphology for this group may also have influenced these results because this acid can carry more hydroxide groups on the surface of the waste during the synthesis process to the other acids, and this may have reduced the interactions between the methylene blue molecules and the adsorbent. This possibility of acid treatment influencing the adsorption of methylene blue in activated carbon was reported by Shaobin Wang *et al.* (2005).

In general, the behavior of the samples from this same group varied little in terms of reactivity among them. Such performance may be associated with hydroxide groups and micropores in similar amounts on the material surface. But the lowest adsorption of methylene blue in PSSUL samples may also have been charged on the surface of the material during acid treatment, which caused little adsorption of negative ions from H_2SO_4 (SO_4^-) on the positive sites on the surface, which leads to the material surface being less negatively charged, thus making it difficult to adsorb positive charge molecules of methylene blue.

However, the adsorption in all the samples occurred in very short intervals of degradation when compared to the average time normally evaluated by studies in the literature which generally report the evolution of the material's reaction with the dye being measured according to the reactivity of the material and the total reaction time being given in hours (Matos *et al.*, 2015). This short reaction time indicates the reaction potential

of the activated carbons produced in the dye adsorption and the high reactivity of the material to wastewater treatment.

The liquid phase adsorption performance of a commercial activated carbon for respiratory protection filter was tested for comparative purposes. The spectrum is shown in Fig. S5 (Supplementary Information). The commercial sample degraded 95% in 5 min. The sample which had similar behavior and slightly superior performance to the commercial product in this study was the PSNIT30 sample, although the commercial sample has a much higher surface area. This confirms the hypotheses in the literature that the surface area and total pore volume are not the only limitations for the adsorption capacity of activated carbons, but also the micropore volume, the charge on the material's surface, the chemical surface of the adsorbates, and the pH of the solutions (Goyal *et al.*, 2001). The surface area had little influence in terms of proportionality of the activator concentration to the adsorption presented by the groups of activated carbon produced in this study.

Therefore, it is believed that the differential performance of carbonized and acidified samples with nitric acid may reveal greater microporous volume and the chemical and electrical interaction effects of the acid on the carbon surface, which affects the adsorption reaction of the material with the dye and ammonia.

One of the main advantages of using activated carbon in adsorbent applications is its post-use. As they are normally produced in burning processes, the repetition of this process makes them suitable for being discarded in nature or even reused, without harming the environment.

4. Conclusions

The simultaneous carbonization–activation process was efficient for the activated carbon production from pumpkin seeds. Activated carbon adsorbed the ammonia gas, but the higher adsorption capacity and selectivity performance at a low temperature was the activated carbon sample activated in 50% nitric acid. The results showed their potential to be used as adsorbent material with this gas. The material was also shown to be suitable for dye adsorption in wastewater with the sample activated in 30% nitric acid. The activated carbons produced in this study are promising materials to be used in cartridges of individual protection equipment for ORP by a sustainable technological method with low cost and which is feasible on an industrial scale.

Authors' contribution

Conceptualization: Silva, W. J.; Andrade Neto, N. F.
Data curation: Silva, W. J.; Andrade Neto, N. F.; Motta, F. V.; Bomio, M. R. D.
Formal analysis: Silva, W. J.; Andrade Neto, N. F.; Ruiz, J. A. C.; Carvalho, F. C.
Funding acquisition: Not applicable.
Investigation: Silva, W. J.; Andrade Neto, N. F.; Carvalho, F. C.
Methodology: Silva, W. J.; Andrade Neto, N. F.; Ruiz, J. A. C.
Project administration: Silva, W. J.; Andrade Neto, N. F.; Longo, E.; Motta, F. V.; Bomio, M. R. D.
Resources: Silva, W. J.; Andrade Neto, N. F.; Carvalho, F. C.; Longo, E.; Motta, F. V.; Bomio, M. R. D.
Software: Silva, W. J.; Ruiz, J. A. C.
Supervision: Silva, W. J.; Ruiz, J. A. C.; Longo, E.; Motta, F. V.; Bomio, M. R. D.
Validation: Not applicable.
Visualization: Not applicable.
Writing – original draft: Silva, W. J.; Andrade Neto, N. F.; Motta, F. V.; Bomio, M. R. D.
Writing – review & editing: Silva, W. J.; Andrade Neto, N. F.; Motta, F. V.; Bomio, M. R. D.

Data availability statement

All data sets were generated or analyzed in the current study

References

Alam, M. Z.; Muyibi, S. A.; Mansor, M. F.; Wahid, R. Activated carbons derived from oil palm empty-fruit bunches: Application to environmental problems. *J. Environ. Sci.* **2007**, *19* (1), 103–108. https://doi.org/10.1016/S1001-0742(07)60017-5

AlOthman, Z. A.; Habila, M. A.; Ali, R.; Ghafar, A. A.; El-din Hassouna, M. S. Valorization of two waste streams into

activated carbon and studying its adsorption kinetics, equilibrium isotherms and thermodynamics for methylene blue removal. *Arab. J. Chem.* **2014**, *7* (6), 1148–1158. https://doi.org/10.1016/j.arabjc.2013.05.007

Bansal, R.; Warrington, A. E.; Gard, A. L.; Ranscht, B.; Pfeiffer, S. E. Multiple and novel specificities of monoclonal antibodies O1, O4, and R-mAb used in the analysis of oligodendrocyte development. *J. Neurosci. Res.* **1989**, *24* (4), 548–557. https://doi.org/10.1002/jnr.490240413

Beuselinck, L.; Govers, G.; Poesen, J.; Degraer, G.; Froyen, L. Grain-size analysis by laser diffractometry: Comparison with the sieve-pipette method. *CATENA* **1998**, *32* (3-4), 193–208. https://doi.org/10.1016/S0341-8162(98)00051-4

Caputi, C. A.; De Carolis, G.; Tomasetti, C. Regional intravenous ketanserin and guanethidine therapy in Raynaud's phenomenon. *Angiology* **1991**, *42* (6), 473–480. https://doi.org/10.1177/000331979104200607

Carvalho, L. M. J.; Gomes, P. B.; Godoy, R. L. O.; Pacheco, S.; Monte, P. H. F.; Carvalho, J. L. V.; Nutti, M. R.; Neves, A. C. L.; Vieira, A. C. R. A.; Ramos, S. R. R. Total carotenoid content, α-carotene and β-carotene, of landrace pumpkins (*Cucurbita moschata* Duch): A preliminary study. *Food Res. Int.* **2012**, *47* (2), 337–340. https://doi.org/10.1016/j.foodres.2011.07.040

Connor, T. H.; MacKenzie, B. A.; DeBord, D. G.; Trout, D. B.; O'Callaghan, J. P. *NIOSH List of Antineoplastic and Other Hazardous Drugs in Healthcare Settings, 2016*; DHHS (NIOSH) Publication No. 2016-161; Department of Health and Human Services, Centers for Disease Control and Prevention, National Institute for Occupational Safety and Health: Washington, DC, 2016. https://www.cdc.gov/niosh/docs/2016-161/pdfs/2016-161.pdf (accessed 2022-03-16).

Dalai, C.; Jha, R.; Desai, V. R. Rice Husk and Sugarcane Baggase Based Activated Carbon for Iron and Manganese Removal. *Aquat. Procedia* **2015**, *4*, 1126–1133. https://doi.org/10.1016/j.aqpro.2015.02.143

Dodevski, V.; Janković, B.; Stojmenović, M.; Krstić, S.; Popović, J.; Pagnacco, M. C.; Popović, M.; Pašalić, S. Plane tree seed biomass used for preparation of activated carbons (AC) derived from pyrolysis. Modeling the activation process. *Colloids Surf. A Physicochem. Eng. Asp.* **2017**, *522*, 83–96. https://doi.org/10.1016/j.colsurfa.2017.03.003

Ferreira, T. A.; Oliveira, C. R.; Chaves, P. P. N.; Milhomens, K. K. B.; Barros, H. B.; Nascimento, I. R. Indução da frutificação paternocárpica de frutos em híbrido de abóbora japonesa com 2, 4-D sob condições de temperatura elevada. *Nucleus* **2017**, *14* (1), 145–152. https://doi.org/10.3738/1982.2278.1686

Gonçalves, A. L.; Rodrigues, C. M.; Pires, J. C. M.; Simões, M. The effect of increasing CO_2 concentrations on its capture, biomass production and wastewater bioremediation by microalgae and cyanobacteria. *Algal Res.* **2016**, *14*, 127–136. https://doi.org/10.1016/j.algal.2016.01.008

Gonzaga, L. C.; Carvalho, J. L. N.; Oliveira, B. G.; Soares, J. R.; Cantarella, H. Crop residue removal and nitrification inhibitor application as strategies to mitigate N2O emissions in sugarcane fields. *Biomass Bioenergy* **2018**, *119*, 206–216. https://doi.org/10.1016/j.biombioe.2018.09.015

Goyal, M.; Rattan, V. K.; Aggarwal, D.; Bansal, R. C. Removal of copper from aqueous solutions by adsorption on activated carbons. *Colloids Surf. A Physicochem. Eng. Asp* **2001**, *190* (3), 229–238. http://doi.org/10.1016/S0927-7757(01)00656-2

Hameed, B. H.; El-Khaiary, M. I. Batch removal of malachite green from aqueous solutions by adsorption on oil palm trunk fibre: Equilibrium isotherms and kinetic studies. *J. Hazard. Mater.* **2008**, *154* (1), 237–244. https://doi.org/10.1016/j.jhazmat.2007.10.017

Huang, H.-j.; Yang, T.; Lai, F.-y.; Wu, G.-q. Co-pyrolysis of sewage sludge and sawdust/rice straw for the production of biochar. *J. Anal. Appl. Pyrolysis* **2017**, *125*, 61–68. https://doi.org/10.1016/j.jaap.2017.04.018

Joshi, D. C.; Das, S. K.; Mukherjee, R. K. Physical properties of pumpkin seeds. *J. Agric. Eng. Res.* **1993**, *54* (3), 219–229. https://doi.org/10.1006/jaer.1993.1016

MacIntyre, C. R.; Chughtai, A. A.; Seale, H.; Richards, G. A.; Davidson, P. M. Respiratory protection for healthcare workers treating Ebola virus disease (EVD): Are facemasks sufficient to meet occupational health and safety obligations? *Int. J. Nurs. Stud.* **2014**, *51* (11), 1421–1426. https://doi.org/10.1016/j.ijnurstu.2014.09.002

Mahamad, M. N.; Zaini, M. A. A.; Zakaria, Z. A. Preparation and characterization of activated carbon from pineapple waste biomass for dye removal. *Int. Biodeterior. Biodegradation* **2015**, *102*, 274–280. https://doi.org/10.1016/j.ibiod.2015.03.009

Marshall, W. E.; Ahmedna, M.; Rao, R. M.; Johns, M. Granular activated carbons from sugarcane bagasse: Production and uses. *Int. Sugar J.* **2000**, *102* (1215), 147–151.

Martins, U. R.; Santos-Silva, A.; Galileo, M. H. M.; Limeira-de-Oliveira, F. Cerambycidae (Coleoptera) dos estados do Piauí e Ceará, Brasil: espécies conhecidas, nova tribo, nova espécie e novos registros. *Iheringia Sér. Zool.* **2014**, *104* (3), 373–384. https://doi.org/10.1590/1678-476620141043373384

Matos, J.; Montaña, R.; Rivero, E., Influence of activated carbon upon the photocatalytic degradation of methylene blue under UV–vis irradiation. *Environ. Sci. Pollut. Res.* **2015,** *22*

(2), 784–791. https://doi.org/10.1007/s11356-014-2832-9

Njoku, K. L.; Akinola, M. O.; Nkemdilim, C. M.; Ibrahim, P. M.; Olatunbosun, A. S. Evaluation of the potentials of three grass plants to remediate crude oil polluted soil. *CAES* **2014**, *2* (4), 131–137.

Nunes, P. H. M. P.; Aquino, L. A.; Santos, L. P. D.; Xavier, F. O.; Dezordi, L. R.; Assunção, N. S. Produtividade do trigo submetido a aplicação de nitrogênio e a inoculação com *Azospirillum brasiliense*. *Ver. Bras. Ci. Solo* **2015**, *39*, 174–182. https://doi.org/10.1590/01000683rbcs20150354

Pezoti Junior, O.; Cazetta, A. L.; Souza, I. P. A. F.; Bedin, K. C.; Martins, A. C.; Silva, T. L.; Almeida, V. C. Adsorption studies of methylene blue onto ZnCl2-activated carbon produced from buriti shells (*Mauritia flexuosa* L.). *J. Ind. Eng. Chem.* **2014**, *20* (6), 4401–4407. https://doi.org/10.1016/j.jiec.2014.02.007

Pezoti, O.; Cazetta, A. L.; Bedin, K. C.; Souza, L. S.; Martins, A. C.; Silva, T. L.; Santos Júnior, O. O.; Visentainer, J. V.; Almeida, V. C. NaOH-activated carbon of high surface area produced from guava seeds as a high-efficiency adsorbent for amoxicillin removal: Kinetic, isotherm and thermodynamic studies. *Chem. Eng. J.* **2016**, *288*, 778–788. https://doi.org/10.1016/j.cej.2015.12.042

Poinern, G. E.; Brundavanam, R.; Le, X. T.; Djordjevic, S.; Prokic, M.; Fawcett, D. Thermal and ultrasonic influence in the formation of nanometer scale hydroxyapatite bio-ceramic. *Int. J. Nanomed.* **2011**, *6*, 2083–2095. https://doi.org/10.2147/IJN.S24790

Rovani, S.; Rodrigues, A. G.; Medeiros, L. F.; Cataluña, R.; Lima, É. C.; Fernandes, A. N. Synthesis and characterisation of activated carbon from agroindustrial waste—Preliminary study of 17β-estradiol removal from aqueous solution. *J. Environ. Chem. Eng.* **2016,** *4* (2), 2128–2137. https://doi.org/10.1016/j.jece.2016.03.030

Shen, L.; Li, Y.; Jiang, L.; Wang, X. Response of Saccharomyces cerevisiae to the Stimulation of Lipopolysaccharide. *PLoS ONE* **2014**, *9* (8), e104428. https://doi.org/10.1371/journal.pone.0104428

Solís-Domínguez, F. A.; Valentín-Vargas, A.; Chorover, J.; Maier, R. M. Effect of arbuscular mycorrhizal fungi on plant biomass and the rhizosphere microbial community structure of mesquite grown in acidic lead/zinc mine tailings. *Sci. Total Environ.* **2011**, *409* (6), 1009–1016. https://doi.org/10.1016/j.scitotenv.2010.11.020

Tsyntsarski, B.; Stoycheva, I.; Tsoncheva, T.; Genova, I.; Dimitrov, M.; Petrova, B.; Paneva, D.; Cherkezova-Zheleva, Z.; Budinova, T.; Kolev, H.; Gomis-Berenguer, A.; Ania, C. O.; Mitov, I.; Petrov, N. Activated carbons from waste biomass and low rank coals as catalyst supports for hydrogen production by methanol decomposition. *Fuel Process.*

Technol. **2015**, *137*, 139–147. https://doi.org/10.1016/j.fuproc.2015.04.016

Van Thuan, T.; Quynh, B. T. P.; Nguyen, T. D.; Ho, V. T. T.; Bach, L. G. Response surface methodology approach for optimization of Cu^{2+}, Ni^{2+} and Pb^{2+} adsorption using KOH-activated carbon from banana peel. *Surf. Interfaces* **2017**, *6*, 209–217. https://doi.org/10.1016/j.surfin.2016.10.007

Wang, S.; Li, L.; Wu, H.; Zhu, Z. H. Unburned carbon as a low-cost adsorbent for treatment of methylene blue-containing wastewater. *J. Colloid Interface Sci.* **2005,** *292* (2), 336–343. https://doi.org/10.1016/j.jcis.2005.06.014

Wang, S.; Gao, B.; Li, Y.; Mosa, A.; Zimmerman, A. R.; Ma, L. Q.; Harris, W. G.; Migliaccio, K. W. Manganese oxide-modified biochars: preparation, characterization, and sorption of arsenate and lead. *Bioresour. Technol.* **2015**, *181*, 13–17. https://doi.org/10.1016/j.biortech.2015.01.044

Wu, L.; Zhang, X.; Liu, D.; Peng, H.; Long, T. Activated Carbons Derived from Livestock Sewage Sludge and their Absorption Ability for the Livestock Sewage. *IERI Procedia* **2014**, *9*, 33–42. https://doi.org/10.1016/j.ieri.2014.09.037

Yorgun, S.; Yıldız, D. Preparation and characterization of activated carbons from Paulownia wood by chemical activation with H_3PO_4. *J. Taiwan Inst. Chem. Eng.* **2015**, *53*, 122–131. https://doi.org/10.1016/j.jtice.2015.02.032

Zhang, S. B.; Lu, Q. Y. Characterizing the structural and surface properties of proteins isolated before and after enzymatic demulsification of the aqueous extract emulsion of peanut seeds. *Food Hydrocoll.* **2015**, *47*, 51–60. https://doi.org/10.1016/j.foodhyd.2015.01.007